Effective spectral densities for system-environment dynamics at conical intersections: S_2–S_1 conical intersection in pyrazine

Rocco Martinazzo [a], Keith H. Hughes [b], Fausto Martelli [a,c], Irene Burghardt [c,*]

[a] Department of Physical Chemistry and Electrochemistry, University of Milan, Via Golgi 19, 20122 Milan, Italy
[b] School of Chemistry, Bangor University, Bangor, Gwynedd LL57 2UW, UK
[c] Département de Chimie, Ecole Normale Supérieure, 24 rue Lhomond, F–75231 Paris cedex 05, France

ABSTRACT

A recently developed effective-mode representation is employed to characterize the influence of a multi-dimensional environment on the S_2–S_1 conical intersection in pyrazine, taken as a paradigm case of high-dimensional dynamics at a conical intersection. We consider a simplified model by which four modes are strongly coupled to the electronic subsystem while a number of weakly coupled tuning modes, inducing energy gap fluctuations, are sampled from a spectral density. The latter is approximated by a series of simplified spectral densities which can be cast into a continued-fraction form, as previously demonstrated in Hughes et al. (K.H. Hughes, C.D. Christ, I. Burghardt, J. Chem. Phys. 131 (2009) 124108). In the time domain, the hierarchy of spectral densities translates to truncated effective-mode chains with a Markovian or quasi-Markovian (Rubin type) closure. A sequential deconvolution procedure is employed to generate this chain representation. The implications for the ultrafast dynamics and its representation in terms of reduced-dimensional models are discussed.

© 2010 Elsevier B.V. All rights reserved.

1. Introduction

Due to the ultrafast time scale which is characteristic of the dynamical events at conical intersection (CoIn) topologies, environmental effects often fall into a distinctly non-Markovian regime. Thus, neither the static limit nor the Markovian limit (assuming rapid fluctuations) are appropriate, making it necessary to explicitly account for the environment's dynamical evolution. Furthermore, due to the multi-dimensional nature of the environment in polyatomic molecules, clusters, or solute-solvent complexes, the topology of the "funnel" region defined by the CoIn can be modified as a function of the environment's structure and dynamics. As a consequence, the boundary between the subsystem and its environment is not necessarily well-defined, and phenomenological models for the environment cannot be expected to be accurate.

In view of the above, a supermolecular perspective including all environmental modes on the same footing as the subsystem modes may seem most appropriate. Various types of such supermolecular approaches have indeed been developed over recent years, including multi-mode vibronic coupling models [1] employed in conjunction with quantum wavepacket dynamics, and quantum-mechanics molecular-mechanics (QM/MM) approaches in conjunction with on-the-fly trajectory-based [2,3] or Gaussian wavepacket-based [4–7] dynamical calculations.

Despite the significant advances in this direction, it is worth investigating whether system-bath theory approaches can provide an alternative perspective, which potentially offers more systematic insight into the influence of the environment on the dynamics and topology. In Refs. [8,9], Markovian system-bath models have thus been employed to model environmental effects on conical intersections. Beyond the Markovian regime, one could conjecture that collective environmental modes can play an important role in the short-time, inertial dynamics. In particular, energy gap fluctuations are expected to translate to a collective solvent coordinate which could guide the dynamics, in line with the Marcus model of charge transfer [10–13]. In the recent developments of Refs. [14–19], this idea has been pursued in view of systematically defining effective modes that characterize the environmental influence upon CoIn's. The present paper connects to and continues these developments.

The effective-mode models developed in Refs. [14–19] interpolate between the supermolecular perspective and conventional system-bath theories, by identifying an explicit but reduced-dimensional representation of the environment. The starting point is a multi-mode vibronic coupling model [1] which describes the coupling of a – high-dimensional or infinite-dimensional – bath to an electronic subsystem, assuming an interaction which is linear

* Corresponding author. Tel.: +33 1 44 32 33 38; fax: +33 1 44 32 33 25.
E-mail address: irene.burghardt@ens.fr (I. Burghardt).

in the bath coordinates. This allows one to introduce collective, Brownian oscillator type modes, similar to the generalized reaction coordinates which have previously been employed in the context of charge transfer processes [10,20]. For conical intersection topologies, $n_{el}(n_{el} + 1)$ effective modes have to be introduced for n_{el} electronic states [14–16] so as to account for the fact that the environment couples both diagonally and off-diagonally to the subsystem. These modes can be shown to fully reproduce the short-time dynamics at the conical intersection [14,15]. Connecting to these developments, one can further introduce chains of effective modes which successively unravel the dynamics as a function of time [17,19,21–23].

In this paper, we apply and further develop the approach of Refs. [22,23] which provides a bridge between the effective-mode picture described above and the conventional description of the environment in terms of spectral densities. For example, assume that the environment gives rise to energy gap fluctuations associated with a spectral density $J(\omega) = \pi/2\sum_n c_n^2/\omega_n\delta(\omega - \omega_n)$ which is determined in terms of frequencies ω_n and vibronic coupling parameters c_n (and which is often available experimentally or by simulations in terms of Fourier transforms of correlation functions). We proceed by approximating $J(\omega)$ in terms of an Mth order continued-fraction expression, which can be shown to correspond to an effective-mode chain terminated by a Markovian closure. From the Mth order model, we successively generate a family of lower-order models involving less effective modes, which, however, still reproduce the dynamics up to a certain time. In practice, complicated spectral densities can be approximated by simpler spectral densities which capture the short-time effects of the environment upon the subsystem accurately. The underlying interpretation is again that few collective modes can be identified which fully describe the effect of the environment on the subsystem dynamics over short-time scales.

In the present paper, we focus on the example of the $S_2(\pi–\pi^*)$–$S_1(n–\pi^*)$ CoIn in pyrazine which has been previously studied in various works by the Munich and Heidelberg groups [24–28]. We construct a model by which an intramolecular or external environment is modeled as a collection of diagonally coupled (tuning type) modes which modulate the subsystem's energy gap, in line with our previous study of Ref. [23]. A more complete treatment would involve fully accounting for the symmetry of the environment modes and for several available system-bath coupling mechanisms – both diagonal and off-diagonal – at the CoIn. A detailed account of these aspects is given in Refs. [29,30].

While a closely related analysis for a tuning mode bath coupled to a nonadiabatic process has been presented in Refs. [23,29], the present paper demonstrates the first application of the general procedure which necessitates approximating an initially given, arbitrary spectral density by an Mth order continued-fraction expression. As detailed below, we have developed a procedure which allows sequential approximations to be carried out in a robust way.

In the remainder of the paper, we first present the relevant CoIn Hamiltonian and spectral densities (Section 2). Following this, reduced effective-mode representations and the associated reduced spectral densities are introduced (Sections 3 and 4). Section 5 presents dynamical results and Section 6 concludes.

2. System-bath Hamiltonian

Along the lines of previous work on the nonadiabatic dynamics in pyrazine [24,26,28] and related vibronic coupling systems [1,27], we consider a multi-mode vibronic coupling Hamiltonian representing the relevant conical intersection including the environment:

$$\hat{H} = \hat{H}_S + \hat{H}_B + \hat{H}_{SB}, \tag{1}$$

where the system part ($\hat{H}_S$) contains the electronic subsystem and a small number of modes which couple strongly to the electronic subsystem, while the bath part ($\hat{H}_B$) is composed of a – potentially very large – number of modes which also couple to the electronic subsystem. In the case of the pyrazine $S_2(\pi–\pi^*)$–$S_1(n–\pi^*)$ CoIn, the system part comprises a subset of four strongly coupled modes [24]. The bath part could correspond either to the remaining intramolecular modes of the polyatomic system (for pyrazine, an intramolecular bath composed of 20 modes) or else could include an external bath with a large or infinite number of degrees of freedom. The system-bath coupling ($\hat{H}_{SB}$) is of purely vibronic type, i.e., the bath modes couple to the electronic system but not among each other, see Eq. (5) below.

2.1. Subsystem Hamiltonian

For the $S_2(\pi–\pi^*)$–$S_1(n–\pi^*)$ CoIn in pyrazine, the subsystem Hamiltonian corresponds to a second-order vibronic coupling model including the coupling mode v_{10a} and three of the totally symmetric modes (v_{6a}, v_1, and v_{9a}) [24]. Parameters were taken from the analysis by Raab et al. [26] which has established a complete second-order model for this CoIn in the full space of 24 normal modes. The system Hamiltonian reads as follows:

$$\hat{H}_S = \hat{V}_A + \sum_{i=1}^{N_S} \left(\frac{1}{2}\hat{p}_{S,i}^2 + \frac{\omega_{S,i}^2}{2}\hat{x}_{S,i}^2\right)\hat{1} + \hat{V}_S(\hat{\boldsymbol{x}}_S), \tag{2}$$

where $\hat{V}_A = -\Delta\hat{\sigma}_z$ gives the electronic splitting, with $\hat{\sigma}_z = |1\rangle\langle1| - |2\rangle\langle2|$ the operator representation of the Pauli matrix, and $\hat{p}_i = (\hbar/i)\partial/\partial x_i$. We use mass-weighted coordinates throughout, differently from the convention of Refs. [14,15,17,21]. The potential part $\hat{V}_S$ represents the coupling of the system modes to the electronic subsystem and is of the form:

$$\hat{V}_S(\hat{\boldsymbol{x}}_S) = \left(\sum_{i\in G_1}\kappa_{S,i}^{(1)}\hat{x}_{S,i} + \sum_{i,j\in G_2}\gamma_{S,ij}^{(1)}\hat{x}_{S,i}\hat{x}_{S,j}\right)\hat{\sigma}_{11}$$

$$+ \left(\sum_{i\in G_1}\kappa_{S,i}^{(2)}\hat{x}_{S,i} + \sum_{i,j\in G_2}\gamma_{S,ij}^{(2)}\hat{x}_{S,i}\hat{x}_{S,j}\right)\hat{\sigma}_{22}$$

$$+ \left(\sum_{i\in G_3}\lambda_{S,i}\hat{x}_{S,i} + \sum_{i,j\in G_4}\mu_{S,ij}\hat{x}_{S,i}\hat{x}_{S,j}\right)(\hat{\sigma}_{12} + \hat{\sigma}_{21}), \tag{3}$$

where $\hat{\sigma}_{nm} = |n\rangle\langle m|$. The Hamiltonian Eq. (3) can alternatively be expressed in terms of the Pauli matrices and the unit matrix, $(\hat{\sigma}_x, \hat{\sigma}_z, \hat{1})$. This form of the potential, in conjunction with the diagonal form of the kinetic energy, corresponds to a (quasi-)diabatic representation [1,31–33].

The relevant subsets of modes in the $(G_1,\ldots,G_4)$ groups are determined from symmetry considerations. The coupled S_2 and S_1 states have B_{3u} and B_{2u} symmetry, respectively. These states are linearly coupled by the v_{10a} mode which is of b_{1g} symmetry; this mode constitutes the G_3 subset in Eq. (3). The modes that couple linearly to the diagonal constitute the G_1 set comprising the a_{1g} modes (v_{6a}, v_1, v_{9a}). The G_2 and G_4 sets involve bilinear combinations of modes whose product is of a_{1g} symmetry (G_2) or of b_{1g} symmetry (G_4), respectively.

Finally, a note of caution is necessary regarding the choice of coordinates, i.e., mass-weighted coordinates as used in Eq. (2), as compared with mass-and-frequency weighted coordinates as previously employed, e.g., in Refs. [15,21]. The effective-mode transformations resulting from these different choices are not identical. Similarly to Refs. [22,23], we prefer to use mass-weighted coordinates in the present context since the kinetic energy is invariant under orthogonal transformations in this

representation, and the bilinear residual bath couplings addressed below are purely of coordinate type. However, it should be pointed out that the moment conservation rules described in Refs. [15,21] have been proven with respect to mass-and-frequency weighted coordinates.

2.2. Bath Hamiltonian and spectral density

In the present model, the bath modes $(\hat{x}_{B,1}, \ldots, \hat{x}_{B,N_B})$, are assumed to couple diagonally to the electronic subsystem, within a linear vibronic coupling (LVC) approximation [1,15]. This is along the lines of the model suggested in Ref. [24], such that the intramolecular bath modes are taken as a collection of tuning modes inducing energy gap fluctuations. While this model is not accurate and realistic in the particular case of pyrazine, since the symmetries of the individual modes are not properly accounted for [26], it will serve here as a vehicle to illustrate the effective-mode techniques addressed below.

The bath Hamiltonian thus reads:

$$\hat{H}_B = \sum_{i=1}^{N_B} \left(\frac{1}{2}\hat{p}_{B,i}^2 + \frac{\omega_{B,i}^2}{2}\hat{x}_{B,i}^2 \right) \hat{1}, \tag{4}$$

and the system-bath coupling is given as

$$\hat{H}_{SB} = \sum_{i=1}^{N_B} \kappa_{B,i}\hat{x}_{B,i}\hat{\sigma}_z, \tag{5}$$

where $\hat{\sigma}_z = \hat{\sigma}_{11} - \hat{\sigma}_{22}$ and $\hat{H}_{SB}$ is of spin-boson form [11].

The couplings $\{\kappa_{B,i}\}$ are sampled from the reference spectral density shown in Fig. 1 (r.h.s. panel). This spectral density was generated from a discrete set of $N_0 = 20$ coupling parameters obtained by Krempl et al. [24] from a weighted random distribution, see the l.h.s. panel of Fig. 1. These couplings relate to the intramolecular bath modes of the pyrazine molecule, assuming that four of the 24 normal modes have been absorbed into the subsystem part, as explained in Section 2.1.

The fitting procedure was based upon a Lorentzian broadening:

$$J(\omega) = \frac{\pi}{2} \sum_{i=1}^{N_0} \frac{\kappa_{B,i}^2}{\omega_{B,i}} \delta(\omega - \omega_{B,i})$$
$$\sim \frac{\pi}{2} \sum_{i=1}^{N_0} \frac{\kappa_{B,i}^2}{\omega_{B,i}} \frac{1}{\pi} \frac{\Delta\omega}{(\omega - \omega_{B,i})^2 + \Delta\omega^2} \tag{6}$$

where $\Delta\omega$ is an equidistant sampling interval. Once the continuous reference spectral density has been generated, it can be re-discretized for an arbitray number of N_B bath modes:

$$J(\omega) = \frac{\pi}{2} \sum_{i=1}^{N_B} \frac{\kappa_{B,i}^2}{\omega_{B,i}} \delta(\omega - \omega_{B,i}). \tag{7}$$

Conversely, the discretized coupling coefficients can be obtained as follows from the spectral density $J(\omega)$, again given an equidistant sampling interval $\Delta\omega$ [22,44]:

$$\kappa_{B,i} = \left(\frac{2}{\pi} J(\omega_{B,i})\omega_{B,i}\Delta\omega \right)^{1/2}. \tag{8}$$

The calculations reported in Section 5 were carried out for $N_B = 20$ bath modes, corresponding to the number of N_0 original data of Ref. [24]. Table 1 reports the relevant frequencies and coupling parameters. The procedure illustrated here is more general, though, and could equally apply to an external environment with a much larger number of modes.

The $\hat{H}_B + \hat{H}_{SB}$ portion of the Hamiltonian is identical to the one addressed in Refs. [22,23], and we will therefore be able to largely draw upon this previous analysis in the following. After recapitulating the main elements of that analysis, we will focus on the application to the spectral density of Fig. 1. The analysis is significantly more challenging than the one of our previous examples since continued-fraction approximants to the realistic spectral density of Fig. 1 are required.

3. Reduced effective-mode representations

We summarize in this section the main steps of the analysis that was previously reported in Refs. [14–18,22,23]. Given a discretized version of the spectral density Eq. (7), the goal of the analysis is (i) to map the environment upon a chain of effective modes which allow one to unfold the system-bath dynamics as a sequential process, and (ii) to construct a reduced-dimensional effective-mode representation of the environment while approximating the residual bath by a Markovian closure. These steps will be detailed in the following, using transformation techniques which we previously introduced. In addition, a novel iterative deconvolution approach will be presented in Section 3.2. These developments are the prerequisite for the spectral density construction which will be addressed in Section 4.
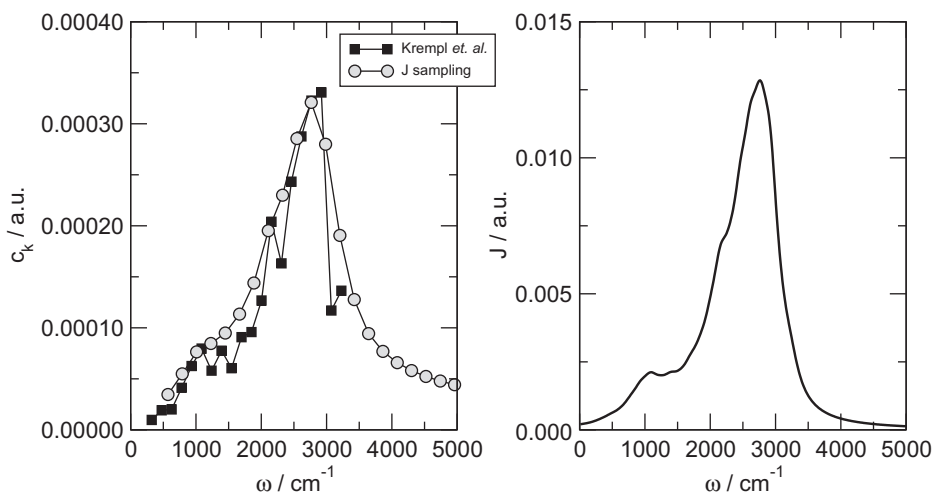

Fig. 1. Left panel: Equidistantly sampled coupling parameters $\{\kappa_{B,i}\}$ (grey circles) based upon the original coupling parameters used by Krempl et al. [24] (black squares) for a 20-mode tuning mode distribution adapted to the S_2–S_1 CoIn in pyrazine. The latter data were smoothed by a Lorentzian broadening and continued to higher frequencies. Right panel: resulting continuous spectral density whose discretization Eq. (7) corresponds to the grey circles of the l.h.s. panel.

Table 1
Sampling frequencies and coupling coefficients of the tuning mode bath employing a 20-mode discretization. The l.h.s. data are taken from Krempl et al. [24] and the r.h.s. data correspond to the reference spectral density depicted in Fig. 1. A frequency spacing of $\Delta\omega = 219.48$ cm^{-1} was used for the reference spectral density data. The 20-mode discretization of the spectral density was employed in the calculations of Section 5, while a finer discretization was used in the representation of the spectral densities in Fig. 2.

Couplings from Krempl et al. [24]		Reference couplings (this work, c.f. Fig. 1)	
ω_n (cm^{-1})	κ_n (a.u.)	ω_n (cm^{-1})	κ_n (a.u.)
322.62	9.72×10^{-6}	570.63	3.47×10^{-5}
475.06	1.92×10^{-5}	790.11	5.49×10^{-5}
627.50	2.00×10^{-5}	1009.58	7.64×10^{-5}
780.75	4.15×10^{-5}	1229.06	8.46×10^{-5}
933.18	6.25×10^{-5}	1448.53	9.49×10^{-5}
1086.43	7.96×10^{-5}	1668.01	1.13×10^{-4}
1238.87	5.80×10^{-5}	1887.48	1.44×10^{-4}
1392.11	7.76×10^{-5}	2106.96	1.95×10^{-4}
1544.55	6.04×10^{-5}	2326.43	2.30×10^{-4}
1697.80	9.08×10^{-5}	2545.91	2.86×10^{-4}
1850.24	9.58×10^{-5}	2765.38	3.21×10^{-4}
2003.48	1.27×10^{-4}	2984.85	2.80×10^{-4}
2155.92	2.04×10^{-4}	3204.33	1.91×10^{-4}
2309.17	1.63×10^{-4}	3423.80	1.28×10^{-4}
2461.60	2.43×10^{-4}	3643.28	9.44×10^{-5}
2614.85	2.88×10^{-4}	3862.75	7.69×10^{-5}
2767.29	3.23×10^{-4}	4082.23	6.58×10^{-5}
2920.53	3.31×10^{-4}	4301.70	5.81×10^{-5}
3072.97	1.17×10^{-4}	4521.18	5.24×10^{-5}
3226.22	1.36×10^{-4}	4740.65	4.79×10^{-5}

3.1. Effective-mode transformations

We focus here on the simplest possible version of the effective-mode transformations described in Refs. [14–16], with a single effective tuning mode which absorbs the system-bath interaction Eq. (5) such that:

$$\widehat{H}_{SB} = \sum_{i=1}^{N_B} \kappa_{B,i} \hat{x}_{B,i} \hat{\sigma}_z \equiv D \widehat{X}_{B,1} \hat{\sigma}_z. \tag{9}$$

This relation defines the first column of an overall coordinate transformation $\widehat{\boldsymbol{X}} = \boldsymbol{T}\hat{\boldsymbol{x}}$. With the requirement of orthogonality of the transformed coordinates, the remainder of the bath Hamiltonian comprising the residual $N_B - 1$ modes has the following structure:

$$\widehat{H}_B = \widehat{H}_B^0 + \widehat{H}_B^{int} \tag{10}$$

with

$$\widehat{H}_B^0 = \sum_{i=1}^{N_B} \left(\frac{1}{2} \widehat{P}_{B,i}^2 + \frac{\Omega_{B,i}^2}{2} \widehat{X}_{B,i}^2 \right) \hat{1}$$

$$\widehat{H}_B^{int} = \sum_{i,j=1}^{N_B} d_{i,j} \widehat{X}_{B,i} \widehat{X}_{B,j} \hat{1} \tag{11}$$

The new frequencies $\{\Omega_{B,i}\}$ and couplings $\{d_{i,j}\}$ result from the coordinate transformation introduced above, such that $\Omega_{B,i}^2 = \sum_{j=1}^{N_B} \omega_{B,j}^2 t_{ji}^2$ and $d_{i,j} = \sum_{k=1}^{N_B} \omega_{B,k}^2 t_{ki} t_{kj}$ where t_{ji} are the elements of the transformation matrix $\boldsymbol{T}$. The residual modes are thus seen to be coupled bilinearly to the effective mode $\widehat{X}_{B,1}$ and among each other, but do not couple directly to the spin subsystem.

Given the above, general form of the transformed bath Hamiltonian $\widehat{H}_B$, several particular realizations can be envisaged, which we now outline. These realizations correspond to different orthogonal transformations, resulting in different intra-chain couplings.

3.1.1. Model 1: secondary bath coupled to primary effective mode

In this case, the bilinear coupling matrix $\{d_{i,j}\}$ is diagonalized in the subspace of the bath modes $\{2,\ldots,N_B\}$ such that only couplings

$\{d_{1,j}\}$ between the primary bath mode $\widehat{X}_{B,1}$ and the secondary bath modes $\widehat{X}_{B,j}, j = 2,\ldots,N_B$, are retained:

$$\widehat{H}_B^{int} = \sum_{i=2}^{N_B} d_{1,i} \widehat{X}_{B,1} \widehat{X}_{B,i} \hat{1}. \tag{12}$$

The secondary modes now act as a bath with respect to the primary mode. The residual couplings $\{d_{1,i}\}$ are entirely determined by the original parameter set and the transformation. They define the residual spectral density:

$$J_{res}^{(1)}(\omega) = \frac{\pi}{2} \sum_{i=2}^{N_B} \frac{d_{1,i}^2}{\Omega_{B,i}} \delta(\omega - \Omega_{B,i}). \tag{13}$$

A particularly simply case is given if the $\{d_{1,i}\}$ conform to an Ohmic spectral density:

$$J_{res}^{(1)}(\omega) = \eta\omega \exp(-\omega/\Lambda), \tag{14}$$

with the friction coefficient η and a suitable cutoff frequency Λ. In this case, the primary bath mode $\widehat{X}_{B,1}$ becomes a simple Brownian oscillator mode whose time evolution is characterized by the complex frequency $\tilde{\Omega}_1 = \Omega_{B,1} - i\eta$ (where the frequency shift induced by the secondary bath has been neglected) [34].

Even if the actual set of residual couplings do not correspond to the spectral density Eq. (14), the Ohmic distribution may be used as an approximation, by which the residual bath is taken to exert a Markovian damping effect.

3.1.2. Model 2: Mori-type chain

In this scheme, the bilinear coupling matrix is cast into a band-diagonal form:

$$\widehat{H}_B^{int} = \sum_{i=1}^{N_B} d_{i,i+1} \widehat{X}_{B,i} \widehat{X}_{B,i+1} \hat{1}. \tag{15}$$

We have referred to this variant as a hierarchical electron-phonon (HEP) model [17–19]. This representation is closely related to a Mori chain [35–37] and to the Rubin model [11,38].

It has been shown in Refs. [15,17,19] that a low-order truncation of the chain will accurately reproduce the short-time dynamics of the system. Higher-order truncation of the band-diagonal (or tridiagonal in this case) form of $\widehat{H}_B^{int}$ successively improves the dynamics as each collective member of the hierarchy is included in the chain. For a bath at zero temperature, this can be shown explicitly in terms of a moment expansion of the Hamiltonian propagator [15,17], leading to the conclusion that at the nth order of the chain (here, n modes), the first $(2n+1)$ Hamiltonian moments are fully determined.

3.1.3. Model 3: truncated Mori-type chain

This variant uses the Mori-type construction of Section 3.1.2 but the hierarchy of modes is now terminated at a chosen order M, such that the bilinear interaction Hamiltonian takes the form:

$$\widehat{H}_B^{int} = \sum_{i=1}^{M-1} d_{i,i+1} \widehat{X}_{B,i} \widehat{X}_{B,i+1} \hat{1} + \widehat{H}_{diss}^{(M)} \tag{16}$$

where $\widehat{H}_{diss}^{(M)}$ corresponds to a residual bath composed of modes $\{M+1,\ldots,N_B\}$ which are all coupled to the Mth mode of the chain:

$$\widehat{H}_{diss}^{(M)} = \sum_{i=M+1}^{N_B} d_{M,i} \widehat{X}_{B,M} \widehat{X}_{B,i} \hat{1}. \tag{17}$$

The Brownian oscillator model of Section 3.1.1 represents a special case of this construction with $M = 1$. Again, the distribution of residual bath modes $(M+1,\ldots,N_B)$ may be approximated in terms of an Ohmic spectral density, see Eq. (14). In this case the picture of a

Mori-type chain with Markovian truncation at the Mth order results.

3.2. Iterative deconvolution approach

In Model 3, the sequential extraction of a series of effective modes from the bath entails that the residual bath space spanning the modes $(M + 1, \ldots, N_B)$ is successively reduced in dimension. If the modes are sampled from a spectral density representing an infinite-dimensional bath rather than a finite-dimensional intramolecular environment, it is desirable, though, to preserve the same bath discretization at every step of the reduction procedure. This can be achieved by an iterative deconvolution approach which is now outlined. The results coincide with those of the tridiagonalization described in Sections 3.1.2 and 3.1.3 if the initial set of modes is large as compared with the relevant subspace of effective modes.

The starting point is again an N_B-dimensional bath obtained by the discretization prescription of Eq. (7). We follow the approach of Model 1, yielding the effective-mode coupling D, frequency $\Omega_{B,1}$, and couplings $d'_{1,i}, i = 2, \ldots, N_B$ to the residual bath modes (here denoted as primed quantities since they are intermediate in the present procedure). The latter conform to the spectral density of Eq. (13).

Differently from the previous transformation approach, we now construct a continuous version of the residual bath spectral density by replacing the δ-functions of Eq. (13) with their Lorentzian approximation. This procedure is entirely analogous to Eq. (6). The resulting continuous spectral density is then re-discretized with the *same* N_B-mode discretization as used for the original bath. The total number of bath modes is thus augmented in each step.

The above procedure is now repeated to yield the successive effective chain couplings and frequencies:

$$d_{i,i}^2 = \sum_{k=1}^{N_B} (d'_{i,k})^2,$$
$$\Omega_{B,i+1}^2 = \frac{1}{d_{i,i}^2} \sum_{k=1}^{N_B} \omega'^2_{B,k} (d'_{i,k})^2, \tag{18}$$

and the corresponding effective modes:

$$\widehat{X}_{B,i+1} = \frac{1}{d_{i,i}} \sum_{k=1}^{N_B} d'_{i,k} \hat{x}'_{B,k} \tag{19}$$

The successive residual bath spectral densities are re-discretized at each step. At the order M, a truncated Mori chain is obtained as in Section 3.1.3, except that the residual bath is not reduced in dimension. This deconvolution procedure has been used below to generate the effective-mode chain parameters. We have verified that the results agree with those obtained from the tridiagonalization approach of Model 3 (Section 3.1.3).

4. Continued-fraction hierarchy of spectral densities

Using the series of approximate bath realizations that are generated from Model 3 or the corresponding deconvolution procedure, leading to an Mth order Mori chain representation with Markovian closure, we now identify the spectral density that each of these realizations is associated with. The family of bath spectral densities that are thus generated define coarse-grained representations of the bath, which lead to an accurate system-bath dynamics over increasing times as the order of the Mori chain is increased. In the following, we explicitly formulate these spectral densities in terms of continued-fraction expressions [22,23]. The derivation is analogous to the one presented in these latter references.

Among the various procedures which can be used to construct spectral densities, we refer here to an approach that expresses the bath-induced relaxation properties of the subsystem in the Heisenberg picture [20,22]. The spectral density $J(\omega)$ can then be defined as follows in terms of the bath-induced portion of the Heisenberg evolution, described by an operator $\widehat{L}_B$:

$$J(\omega) = \lim_{\epsilon \to 0^+} \mathrm{Im} \widehat{L}_B(z) \Big|_{z = \omega - i\epsilon}, \tag{20}$$

where $\widehat{L}_B(z)$ determines the dissipative evolution of the subsystem Heisenberg operators in a Fourier/Laplace transformed representation. Eq. (20) corresponds to the definition of the spectral density as the imaginary part of the dynamic susceptibility [10,20].

If only a single system-bath interaction mechanism is involved, as is the case in the situation studied here, the nature of the subsystem operators is not of importance and one can formally replace an arbitrary subsystem operator by the coordinate operator [20,22]. Exact Laplace-domain equations can then be obtained as detailed in Ref. [22], leading to a continued-fraction (CF) representation of $\widehat{L}_B(z)$. The latter can be truncated at successive orders so as to generate a series of approximate effective-mode chains which correspond to Mth order CF's of the following form [22]:

$$\widehat{L}_B^{(M)}(z) = -\cfrac{D^2}{\Omega_1^2 - z^2 - \cfrac{d_{1,2}^2}{\Omega_2^2 - z^2 - \cdots \cfrac{d_{M-2,M-1}^2}{\Omega_{M-1}^2 - z^2 - \cfrac{d_{M-1,M}^2}{\Omega_M^2 - z^2 - z^2 I^{(M)}(z)}}}}, \tag{21}$$

where the closure function $I^{(M)}(z)$ is defined as

$$I^{(M)}(z) = \sum_{k=1}^{N} \frac{c_k^2}{\omega_k^2(\omega_k^2 - z^2)} \simeq \frac{2}{\pi} \int_0^\infty d\omega \frac{J_{\mathrm{res}}^{(M)}(\omega)}{\omega(\omega^2 - z^2)}, \tag{22}$$

with the Mth order residual spectral density $J_{\mathrm{res}}^{(M)}$. In the following, two choices for approximate residual spectral densities and the associated closure functions are addressed, i.e., an Ohmic residual bath as is Eq. (14), and the quasi-Ohmic closure introduced by Rubin [11,38] in the construction of an oscillator chain model which is a special case of the present one.

Using Eqs. (20)–(22), an Mth order reduced spectral density can be defined by analogy with Eq. (20):

$$J^{(M)}(\omega) = \lim_{\epsilon \to 0^+} \mathrm{Im} \widehat{L}_B^{(M)}(z) \Big|_{z = \omega - i\epsilon}. \tag{23}$$

These Mth order approximants to the spectral density are the central object under study in the remainder of the paper.

4.1. Ohmic closure

The Ohmic closure has already been defined in Eq. (14) in the discussion of Model 1, and corresponds to the spectral density $J_{\mathrm{res}}^{(M)}(\omega) = \eta \omega \exp(-\omega/\Lambda)$ where η is the friction coefficient of the corresponding Langevin description and Λ is the frequency cutoff. The closure function Eq. (22) takes the following form in the Ohmic case:

$$I_{\mathrm{ohm}}(z) = -i \frac{\eta}{z}. \tag{24}$$

With I_{ohm}, the first order $M = 1$ of Eqs. (21)–(23) yields a Lorentzian form, as previously obtained by Garg et al. [20,22]:

$$J^{(1)}(\omega) = \frac{\eta \omega D^2}{\left(\Omega_1^2 - \omega^2\right)^2 + \eta^2 \omega^2}. \tag{25}$$

The second order can also be obtained analytically [22]:

$$J^{(2)}(\omega) = \frac{D^2\left[\left(\Omega_2^2 - \omega^2\right)^2 + \eta^2\omega^2\right]\eta\omega d_{1,2}^2}{A^2(\omega) + B^2(\omega)}, \tag{26}$$

where $A(\omega)$ and $B(\omega)$ are the $\epsilon \to 0^+$ limits of $A(z) = (\Omega_1^2 - z^2)$ $|\hat{L}_2(z)|^2 - d_{12}^2 \, Re \, \hat{L}_2(z)$ and $B(z) = d_{12}^2 Im\hat{L}_2(z)$, with $\hat{L}_2(z) = \Omega_2^2 - z^2 + i\eta z$.

4.2. Rubin closure

In the Rubin model [11,38], the residual spectral density takes the quasi-Ohmic form:

$$J_{res}^{(M)}(\omega) = \frac{\omega\Lambda_R}{2}\left(1 - \frac{\omega^2}{\Lambda_R^2}\right)^{1/2}\Theta(\Lambda_R - \omega), \tag{27}$$

where Θ is the Heaviside step function and Λ_R is a cutoff frequency. The closure function is now given as

$$I_{Rubin}(z) = \frac{1}{2z}\frac{\Lambda_R^2 - 2z^2 + 2iz\sqrt{\Lambda_R^2 - z^2}}{z + i\sqrt{\Lambda_R^2 - z^2}}. \tag{28}$$

Comparison with the Ohmic case corresponds to equating $\Lambda_R = 2\eta$; however, the Rubin cutoff frequency is fixed by the frequency range employed in the numerical discretization, $\Lambda_R = N\Delta\omega$.

In the numerical construction of the reduced spectral densities $J^{(M)}$ described in the next section, the Rubin closure proved significantly more stable than the Ohmic closure in the limit $\epsilon \to 0^+$.

4.3. Application to model spectral density

In Fig. 2, Eqs. (21)–(23) were applied in conjunction with the Rubin closure in order to generate a family of approximate spectral densities approaching the reference spectral density of Fig. 1. The reference spectral density (r.h.s. of Fig. 1) was re-discretized according to Eq. (7) for a large number of points, between $N_B = 250$ and $N_B = 1000$. The iterative deconvolution procedure of Section 3.2. was then applied in order to obtain the chain parameters. For this large number of points, the band diagonalization procedure of Section 3.1.3 (Model 3) was shown to yield very similar results. Finally, Eqs. (21)–(23) in conjunction with the Rubin closure of Section 4.2 were employed to generate the Mth order CF approximants shown in the figure.

Fig. 2 illustrates that the lowest-order approximants $J^{(M)}$, $M = 1$, 2, are not centered on the reference spectral density, even though

their construction guarantees that they reproduce the short-time dynamics. In this sense, the $J^{(M)}$'s cannot be understood as simple coarse-grained versions of the actual spectral density. From $M = 3$ onwards, the successive approximants coincide more closely with the center of the reference spectral density and tend to converge. The $M = 15$ case is a rather good approximation, even though it is not converged yet. At higher orders, e.g., $M = 100$, oscillatory features appear which are presumably numerical artifacts and should be eliminated in a more refined procedure.

Overall, the present analysis shows that convergence at the level of the spectral densities necessitates relatively high orders in the CF development. In the following, the convergence of the Mth order approximations will be considered from the complementary time-domain viewpoint. Here, one would expect more rapid convergence since the effective-mode procedure is designed as an expansion in the time domain.

5. System-bath dynamics for the S_2–S_1 CoIn in pyrazine

In line with the model Hamiltonian described in Section 2, the reference spectral density of Fig. 1 is now taken to represent a tuning mode bath that is coupled to a 4-mode subsystem model of the S_2–S_1 conical intersection in pyrazine, described according to the second-order vibronic coupling Hamiltonian of Raab et al. [26]. As explained in Section 2, a linear vibronic coupling approximation is only made for the bath part.

From the above discussion, two approaches can be followed for carrying out the dynamics at a given level M of the effective-mode hierarchy: (i) In the first approach, the transformed representation of the Hamiltonian is employed and M effective modes are included in the dynamical calculation, along with the residual bath which is treated at the level of an Ohmic or quasi-Ohmic (Rubin) closure. Here, the residual bath is treated either implicitly, by a master equation, or else explicitly in terms of a discretized, finite-dimensional representation [22,23]. (ii) In the second approach, the reduced spectral densities of Section 4 are employed, which can be discretized in the same way as the original spectral density. In both approaches, a reduced-dimensional representation of the bath is aimed at, which is realized in the first case by employing few effective modes, and in the second case by simplified low-order spectral densities. At a formal level, the approaches (i) and (ii) are equivalent.

While we have followed the approach (i) in a number of applications [14–19], we demonstrate here the second approach, with
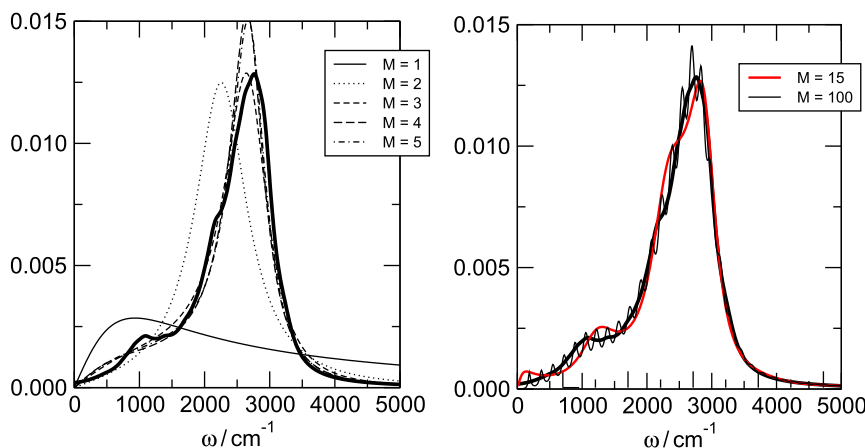

Fig. 2. Spectral densities $J^{(M)}(\omega)$, $M = 1,\ldots,5$, $M = 15$, and $M = 100$, approaching the reference spectral density of Fig. 1, which is also shown in both panels (solid black line). The successive $J^{(M)}$ approximants are generated from Eq. (23) employing the Rubin closure of Section 4.2. The CF parameters were obtained from the reference spectral density by employing the iterative deconvolution procedure of Section 3.2.

the aim of testing the time-domain convergence of the spectral densities shown in the preceding section.

All calculations are carried out for the combined subsystem plus bath at zero temperature, using the multiconfiguration time-dependent Hartree (MCTDH) method [39–42] and employing basis sets similar to those specified for previous calculations for the same type of system [26–28]. Initial conditions correspond to the Franck–Condon geometry, which is also the reference geometry for the Taylor expansion underlying the vibronic coupling model of Section 2. We choose a discretization for $N_B = 20$ bath modes, which together with the 4-mode subsystem can be taken to correspond to the 24 normal modes of pyrazine. However, while the perspective developed here can be applied to a finite-dimensional intramolecular bath, it is equally suitable to describe an external bath with a large or infinite number of degrees of freedom. As is clear from the preceding section, the procedure can be straightforwardly extended to an arbitrary number of modes sampled from a given spectral density. Since the relevant observation time scale is short, of the order of 100 femtoseconds, the dynamics induced by the discretized bath is effectively irreversible.

The reference spectral density of Fig. 1 as well as the $M = 1, \ldots, 3$ approximants of Fig. 2 are discretized in exactly the same fashion for $N_B = 20$ bath modes, see Fig. 3. Table 2 summarizes the parameters determining the corresponding Mth order CF approximants. Time-dependent calculations for the different realizations of the spectral density were then compared, as illustrated in Fig. 4. The figure shows the time-evolving S_2 diabatic state populations along with the wavepacket autocorrelation function $|C(t)| = |\langle \psi(0)|\psi(t)\rangle|$. For comparison, results for the bare 4-mode system are shown, which features significantly stronger recurrences and a different population dynamics.

All calculations reported in Fig. 4 agree on the shortest time scale (~5 fs), and the orders $M = 2, 3$ are found to be very close over

the complete observation interval. The $M = 3$ result is virtually indistinguishable from the result obtained from the reference spectral density and can be considered as converged. The $M = 1$ order gives a qualitatively correct picture of the dynamics, which is intermediate between the bare subsystem dynamics and the full dynamics over the whole observation interval. The results shown here are qualitatively similar to the preliminary analysis presented in Ref. [29].

The fact that convergence in the time domain is achieved already at the order $M = 3$ may seem surprising, given that the corresponding spectral density is far from converged as far as the detailed frequency-domain structure goes, see Figs. 2 and 3. The reason lies in the short time scale of the relevant decay process, over which the details of the bath spectral density cannot be fully resolved.

6. Discussion and conclusions

To summarize, we have illustrated a general procedure for the systematic reduction of environmental spectral densities within the framework of a vibronic coupling model. Following our earlier developments [22,23], a family of approximate spectral densities are generated, which are sequentially resolved by the subsystem in the course of the dynamics. The model presented here is in line with the concept of Refs. [14–16] where the subsystem is represented by a vibronic coupling model of higher than linear order, while the bath part is restricted to the LVC level of treatment. The bath is thus amenable to the effective-mode transformations detailed above.

The hierarchy of spectral densities presented here originates in the effective-mode transformation approach, but goes beyond these developments in that it abstracts from the discrete nature of the environment. Instead, the reduction is achieved at the level of the CF representation of the continuous spectral densities of Eqs. (21)–(23). This framework is best suited to a system-bath theory perspective. Indeed, the use of the Markovian or quasi-Markovian (Rubin) closure of Section 4, which underlies the spectral density construction, implies that no artifacts appear due to the truncation of the effective-mode chain. The excitation thus cannot "propagate back" along the chain, and an irreversible dynamics results. This is in contrast to the effective-mode approximations which were carried out in the analyses of Refs. [14–16,19] for finite-dimensional polyatomic systems.

The perspective resulting from the present analysis is that the subsystem sequentially resolves the environment's spectral density as time proceeds. Thus, at short times the subsystem sees a coarse-grained view of the environment, with a spectral density that corresponds to a low-order continued-fraction representation (note, though, that these coarse-grained versions do not simply involve a coarse-graining in the frequency domain, see Section 4.3). Successive higher-order CF's approach the true spectral density. In keeping with Refs. [22,23], the present analysis underscores the formal equivalence between approximate CF spectral densities and truncated Mori chain representations, i.e., effective-mode chains with (quasi-) Markovian closure. While this relation
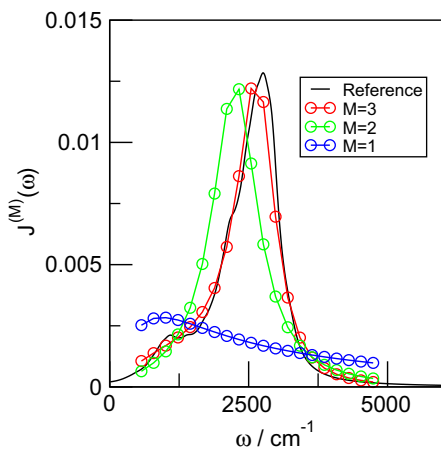

Fig. 3. Lowest-order spectral density approximants $J^{(M)}(\omega)$, $M = 1, \ldots, 3$, as compared with the reference spectral density of Fig. 1 (black line). The Mth order spectral densities correspond to those shown in Fig. 2, but exhibit a coarser discretization, using 20 frequency-domain points. This discretization has been employed in the dynamical calculations illustrated in Fig. 4.

Table 2
Effective-mode parameters for the closure levels $M = 1, 2, 3$. The effective-mode frequencies are quoted in cm^{-1} and the $d_{n-1,n}$ coupling terms are quoted in atomic units. The friction coefficient η is defined in terms of the cutoff frequency of the Rubin model, $\eta = \Lambda_R/2$ (Section 4.2), where $\Lambda_R = N\Delta\omega$ is determined by the discretization employed in the deconvolution procedure of Section 3.2.

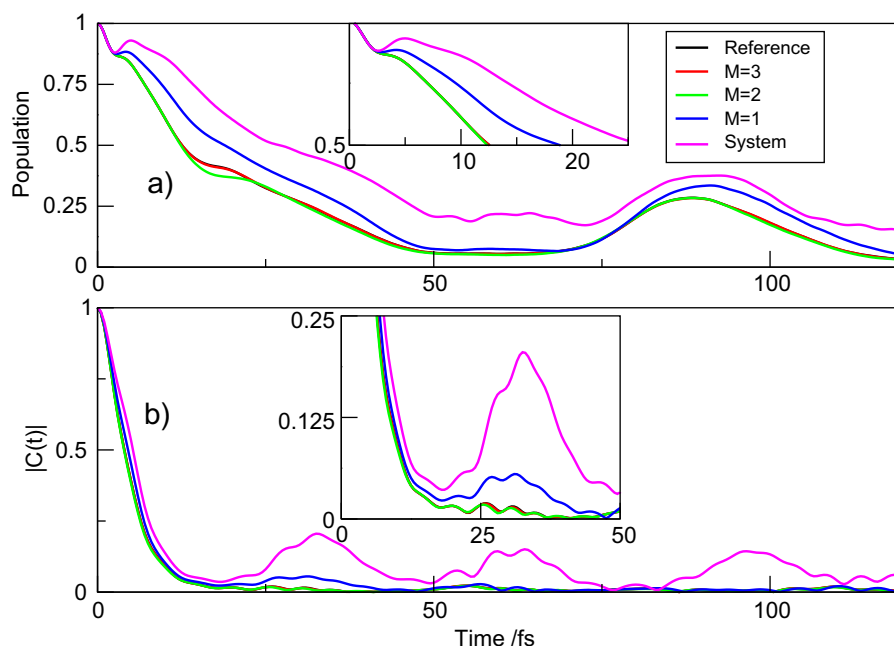| M	Ω_{B1}	Ω_{B2}	Ω_{B3}	d_{01}	d_{12}	d_{23}	η (a.u.)
3	3035.25	8539.05	4756.33	7.18×10^{-4}	2.27×10^{-4}	6.71×10^{-4}	0.055
2	3035.25	5170.96	NA	7.18×10^{-4}	2.27×10^{-4}	NA	0.108
1	2174.77	NA	NA	7.18×10^{-4}	NA	NA	0.152

Fig. 4. Upper panel: time dependence of the S_2 state (diabatic) population for successive 4 + 20-mode models based on the bath spectral densities $J^{(M)}, M = 1,2,3$ illustrated in Fig. 3. Lower panel: time dependence of the wavepacket autocorrelation function (absolute value), $|C(t)| = |\langle\psi(0)|\psi(t)\rangle|$. For comparison, results for the bare subsystem dynamics are also shown.

connects to various previous results in the literature [35–37], its implications have not been previously explored in the context of high-dimensional quantum dynamics.

In the present work, the focus has been on demonstrating the equivalence between the truncated effective-mode chains and the reduction at the level of the associated spectral densities. The calculations reported in Section 5 in fact did not involve a reduction in the number of sampling points as compared with the reference spectral density. The general prescription to be followed in view of a true reduced-dimensional dynamics involves the transformed, effective-mode representation and the treatment of the residual bath at an implicit level, e.g., involving master equations [22,23]. Indeed, the effective-mode picture offers a unique "minimal discretization" of the bath.

Even though convergence can be analyzed with respect to both the frequency and time-domain perspective, the present application illustrates that time-domain convergence remains the most natural viewpoint, since the effective-mode chains represent a perturbation theory in time. Furthermore, the fast processes under consideration favor a rapid convergence of the effective-mode expansion. Thus, in the example discussed above, the $M = 3$ approximant is found to yield a converged dynamics even though the corresponding spectral density is still perceptibly different from the reference spectral density. Indeed, the effective-mode approach is ideally tailored to the ultrafast dynamics at CoIn's, where the chain representation is expected to converge rapidly. For an arbitrary, possibly complicated spectral density constructed, e.g., from molecular dynamics (MD) simulations, we conjecture that the lowest-order approximants will capture the dominant effects of the environment on the CoIn dynamics.

Beyond the present level of analysis, we will formally demonstrate in a forthcoming publication [43] that the present approach is of considerable generality and systematically converges for arbitrary baths. The present reduction procedure thus offers a general approach for deconvoluting complicated, structured spectral densities in terms of an underlying collective mode ensemble.

Finally, the case addressed here, i.e., a tuning mode bath giving rise to energy gap fluctuations, covers many physically relevant sit-

uations, but is restricted in that the environment is taken to couple only diagonally to the CoIn. The more general case where the environmental modes couple both diagonally ($\propto \hat{\sigma}_z$) and off-diagonally ($\propto \hat{\sigma}_x$), has been addressed in Refs. [29,30]. In these references, we also considered simultaneous bath couplings to several subsystem operators, which necessitates a generalization of the present treatment to cross-correlated spectral densities.

We expect the effective-mode models described here to be versatile tools that can predict general trends, and that can be used in conjunction with microscopic information provided from other sources, e.g., spectral densities, energy gap correlation functions, etc. Further, model parametrizations could be provided by QM/MM type simulations, and the model-based dynamics could be employed to analyse the wealth of microscopic information provided by such simulations. Such complementary strategies would bridge the gap between system-bath theory approaches and explicit multi-dimensional simulations for ultrafast photochemical processes in various types of environments.

Acknowledgments

References

[1] H. Köppel, W. Domcke, L.S. Cederbaum, Adv. Chem. Phys. 57 (1984) 59.
[2] G. Groenhof, M. Bouxin-Cademartory, B. Hess, S.P. de Visser, H.J.C. Berendsen, M. Olivucci, A.E. Mark, M.A. Robb, J. Am. Chem. Soc. 126 (2004) 4228.
[3] M. Boggio-Pasqua, M.A. Robb, G. Groenhof, J. Am. Chem. Soc. 131 (2009) 13580.
[4] A. Toniolo, S. Olsen, L. Manohar, T.J. Martínez, Faraday Discuss. Chem. Soc. 127 (2004) 149.
[5] A.M. Virshup, C. Punwong, T.V. Pogorelov, B.A. Lindquist, C. Ko, T.J. Martínez, J. Phys. Chem. B 113 (2009) 3280.
[6] B.G. Levine, T.J. Martínez, Annu. Rev. Phys. Chem. 58 (2007) 613.
[7] G.A. Worth, M.A. Robb, I. Burghardt, Faraday Discuss. 127 (2004) 307.
[8] A. Kühl, W. Domcke, J. Chem. Phys. 116 (2002) 263.
[9] D. Gelman, G. Katz, R. Kosloff, M.A. Ratner, J. Chem. Phys. 123 (2005) 134112.

[10] S. Mukamel, Principles of Nonlinear Optical Spectroscopy, Oxford University Press, New York, Oxford, 1995.

[11] U. Weiss, Quantum Dissipative Systems, World Scientific, Singapore, 1999.

[12] R.A. Marcus, N. Sutin, Biochim. Biophys. Acta 811 (1985) 265.

[13] A. Nitzan, Chemical Dynamics in Condensed Phases, Oxford University Press, New York, Oxford, 2006.

[14] L.S. Cederbaum, E. Gindensperger, I. Burghardt, Phys. Rev. Lett. 94 (2005) 113003.

[15] E. Gindensperger, I. Burghardt, L.S. Cederbaum, J. Chem. Phys. 124 (2006) 144103.

[16] I. Burghardt, E. Gindensperger, L.S. Cederbaum, Mol. Phys. 104 (2006) 1081.

[17] H. Tamura, E.R. Bittner, I. Burghardt, J. Chem. Phys. 126 (2007) 021103.

[18] H. Tamura, J. Ramon, E.R. Bittner, I. Burghardt, J. Phys. Chem. B 112 (2008) 495.

[19] E. Gindensperger, H. Köppel, L.S. Cederbaum, J. Chem. Phys. 126 (2007) 034106.

[20] A. Garg, J.N. Onuchic, V. Ambegaokar, J. Chem. Phys. 83 (1985) 4491.

[21] H. Tamura, E.R. Bittner, I. Burghardt, J. Chem. Phys. 127 (2007) 034706.

[22] K.H. Hughes, C.D. Christ, I. Burghardt, J. Chem. Phys. 131 (2009) 024109.

[23] K.H. Hughes, C.D. Christ, I. Burghardt, J. Chem. Phys. 131 (2009) 124108.

[24] S. Krempl, M. Winterstetter, H. Plöhn, W. Domcke, J. Chem. Phys. 100 (1994) 926.

[25] G.A. Worth, H.-D. Meyer, L.S. Cederbaum, J. Chem. Phys. 109 (1998) 3518.

[26] A. Raab, G.A. Worth, H.-D. Meyer, L.S. Cederbaum, J. Chem. Phys. 110 (1999) 936.

[27] G.A. Worth, H.-D. Meyer, H. Köppel, L.S. Cederbaum, I. Burghardt, Int. Rev. Phys. Chem. 27 (2008) 569.

[28] I. Burghardt, K. Giri, G.A. Worth, J. Chem. Phys. 129 (2008) 174104.

[29] I. Burghardt, K.H. Hughes, H. Tamura, E. Gindensperger, H. Köppel, L.S. Cederbaum, in: D.R. Yarkony, H. Köppel, W. Domcke, (Eds.), Conical Intersections, Theory, Computation and Experiment, World Scientific, New Jersey, 2010, in press.

[30] I. Burghardt, K.H. Hughes, Effective-mode representation of non-Markovian dynamics: a hierarchical approximation of the spectral density. III. Application to conical intersections, J. Chem. Phys., submitted for publication.

[31] G.A. Worth, L.S. Cederbaum, Annu. Rev. Phys. Chem. 55 (2004) 127.

[32] H. Köppel, W. Domcke, L.S. Cederbaum, in: W. Domcke, D.R. Yarkony, H. Köppel (Eds.), Conical Intersections, vol. 15, World Scientific, New Jersey, 2004, p. 323.

[33] H. Köppel, W. Domcke, Encyclopedia in Computational Chemistry, Wiley, New York, 1998. p. 3166.

[34] N.G. van Kampen, Stochastic Processes in Physics and Chemistry, North-Holland, Amsterdam, 1992.

[35] H. Mori, Prog. Theor. Phys. 34 (1965) 399.

[36] M. Dupuis, Prog. Theor. Phys. 37 (1967) 502.

[37] P. Grigolini, G.P. Parravicini, Phys. Rev. B 25 (1982) 5180.

[38] R.J. Rubin, Phys. Rev. 131 (1963) 964.

[39] H.-D. Meyer, U. Manthe, L.S. Cederbaum, Chem. Phys. Lett. 165 (1990) 73.

[40] U. Manthe, H.-D. Meyer, L.S. Cederbaum, J. Chem. Phys. 97 (1992) 3199.

[41] M.H. Beck, A. Jäckle, G.A. Worth, H.D. Meyer, Phys. Rep. 324 (2000) 1.

[42] G.A. Worth, M.H. Beck, A. Jäckle, H. Meyer, The MCTDH Package, Version 8.2 (2000), 2006.;
H.-D. Meyer, Version 8.3 (2002). <http://www.pci.uni-heidelberg.de/tc/usr/mctdh/>, 2006.

[43] R. Martinazzo, B. Vacchini, K.H. Hughes, I. Burghardt, submitted for publication.

[44] M. Nest, H.-D. Meyer, J. Chem. Phys. 24 (2003) 119.